JOURNAL OF VIROLOGY, Feb. 1999, p. 1503–1517 Vol. 73, No. 2
0022-538X/99/$04.00+0

Vaccinia Virus Intracellular Mature Virions Contain only One Lipid Membrane

MICHAEL HOLLINSHEAD, ALAIN VANDERPLASSCHEN, GEOFFREY L. SMITH, AND DAVID J. VAUX*

Sir William Dunn School of Pathology, University of Oxford, Oxford OX1 3RE, United Kingdom

Received 6 October 1998/Accepted 2 November 1998

Vaccinia virus (VV) morphogenesis commences with the formation of lipid crescents that grow into spherical immature virus (IV) and then infectious intracellular mature virus (IMV) particles. Early studies proposed that the lipid crescents were synthesized de novo and matured into IMV particles that contained a single lipid bilayer (S. Dales and E. H. Mosbach, Virology 35:564–583, 1968), but a more recent study reported that the lipid crescent was derived from membranes of the intermediate compartment (IC) and contained a double lipid bilayer (B. Sodiek et al., J. Cell Biol. 121:521–541, 1993). In the present study, we used high-resolution electron microscopy to reinvestigate the structures of the lipid crescents, IV, and IMV particles in order to determine if they contain one or two membranes. Examination of thin sections of Epon-embedded, VV-infected cells by use of a high-angular-tilt series of single sections, serial-section analysis, and high-resolution digital-image analysis detected only a single, 5-nm-thick lipid bilayer in virus crescents, IV, and IMV particles that is covered by a 8-nm-thick protein coat. In contrast, it was possible to discern tightly apposed cellular membranes, each 5 nm thick, in junctions between cells and in the myelin sheath of Schwann cells around neurons. Serial-section analysis and angular tilt analysis of sections detected no continuity between virus lipid crescents or IV particles and cellular membrane cisternae. Moreover, crescents were found to form at sites remote from IC membranes—namely, within the center of virus factories and within the nucleus—demonstrating that crescent formation can occur independently of IC membranes. These data leave unexplained the mechanism of single-membrane formation, but they have important implications with regard to the mechanism of entry of IMV and extracellular enveloped virus into cells; topologically, a one-to-one membrane fusion suffices for delivery of the IMV core into the cytoplasm. Consistent with this, we have demonstrated previously by confocal microscopy that uncoated virus cores within the cytoplasm lack the IMV surface protein D8L, and we show here that intracellular cores lack the surface protein coat and lipid membrane.

Vaccinia virus (VV) is a large, much-studied member of the *Poxviridae* that is unusual among DNA viruses in that it completes both DNA replication and virus assembly in the cytoplasm of infected cells (21). Replication and assembly occur in viral factories, discrete, virus-induced cytoplasmic structures from which cellular organelles are excluded (7, 17, 19), although the factories are often closely surrounded by endoplasmic reticulum (ER). Assembly begins with the appearance of membrane crescents deep within the virus factories. These structures contain an array of spicules attached to the convex surface and extend to form spherical immature virions (IV), from which the first infectious progeny, the intracellular mature virions (IMV), are formed by a series of maturation steps including proteolysis (22).

IMV represent the majority of infectious progeny, but some IMV become enveloped by two membranes (15, 25), derived from the Golgi complex (13, 30) or early endosomes (38), to form intracellular enveloped virus (IEV) particles. The IEV may induce the polymerization of actin (4) and move to the cell surface, where the outer membrane fuses with the plasma membrane, forming extracellular enveloped virus (EEV), which is either released from the cell or retained at the cell surface as cell-associated enveloped virus (1).

The origin of the membrane of crescents and IVs is not immediately apparent. Early electron-microscopic studies were unable to identify connections between the nascent crescent membrane and any host intracellular membrane, leading to the proposal that the membrane did not derive from a preexisting host organelle but arose by a novel de novo synthesis (5). More recently, this view was challenged by results obtained from frozen-section, cryo-, and immunoelectron-microscopic studies (34). These results were interpreted as indicating that the crescent membrane consists of a tightly apposed pair of host cell membranes derived from an exocytic compartment, intermediate between the ER and the Golgi apparatus, termed the intermediate compartment (IC). However, electron microscopy of Epon-embedded sections did not reveal two lipid membranes. Sometimes separation of two layers at the surface of IMV was apparent if the infected cell or isolated IV was treated first with a protease or reducing agent (34).

Since biological membranes have a common general structure, consisting of lipid and protein molecules, with the lipid molecules arranged as a continuous double layer (31), we reasoned that it should be possible to differentiate between a single membrane and a tightly apposed pair of membranes. By conventional electron microscopy, the unit cellular membrane appears extremely thin, characteristically approximately 5 nm thick. In conventional plastic sections, staining of the lipid bilayer (by osmium and heavy metals) is observed primarily over the polar regions of phospholipid molecules, causing them to appear electron dense, whereas the center of the membrane appears translucent, giving a trilaminar profile with positive contrast. An alternative method uses thawed frozen sections, in which lipid bilayers exclude totally the heavy metal stains used for contrasting. Cellular membranes still appear as

* Corresponding author. Mailing address: Sir William Dunn School of Pathology, University of Oxford, S. Parks Rd., Oxford OX1 3RE, United Kingdom. Phone: 44 1865 275544. Fax: 44 1865 275501. E-mail: Vaux@molbiol.ox.ac.uk.

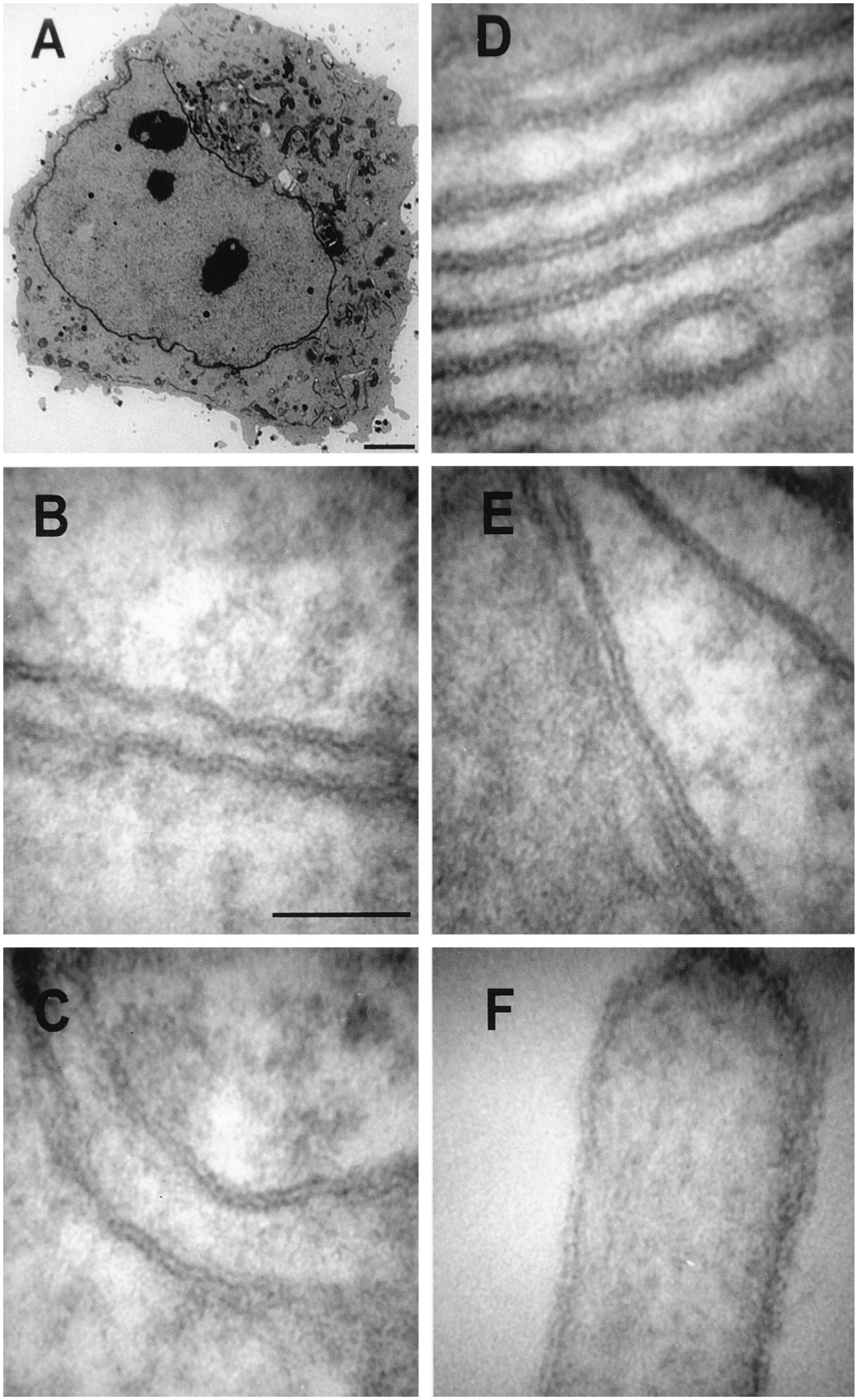

FIG. 1. Conventional electron-microscopic analysis of VV-infected HeLa cell. (A) Low-magnification view of a HeLa cell infected with VV strain WR for 16 h. Virus factories are evident on both side of the nucleus, and Golgi cisternae are located on only one side of the nucleus. (B to F) Images of the nuclear envelope (B), rough ER (C), Golgi cisternae (D), mitochondrial membrane (E), and microvillus (plasma membrane) (F), captured at a primary magnification of ×250,000, from the infected cell shown in panel A. Measurements of membrane thickness for each organelle were performed on the digital images, using the SIS analysis program Esivision (Table 1). Bars: 2.5 μm (A) and 50 nm (B to F).

TABLE 1. Thicknesses of the membranes of cellular organelles and the IV form of VV, measured by conventional electron microscopy of VV-infected HeLa cells

Structure	Mean bilayer thickness ± SD, nm (n = 10)
Nuclear envelope	5.07 ± 0.19
ER	5.15 ± 0.12
Golgi membrane	5.19 ± 0.22
Mitochondrial membrane	4.97 ± 0.25
Plasma membrane	4.97 ± 0.20
IV membrane	5.04 ± 0.24

5-nm profiles, but now they are electron translucent and have negative contrast (37). The underlying organizations of host cell membranes utilized for viral assembly would be expected to be similar.

In this study, we examined VV-infected cells by transmission electron microscopy, using a combination of tilt series and serial-section analysis with digital-image acquisition and image processing to study the formation and morphology of the membrane structure associated with IV and IMV. Multiple lines of evidence show that the virus crescent membrane and IV membrane are not continuous with the IC and that the IMV is enveloped in a single membrane comprising a conventional lipid bilayer and a prominent asymmetric protein coat.

MATERIALS AND METHODS

Cells and virus. HeLa cells were grown in Dulbecco's modified Eagle medium (Gibco) containing 10% heat-inactivated fetal bovine serum. RK_{13} cells were grown in minimum essential medium with 10% fetal bovine serum. Cells were infected with one of two VV strains, Western Reserve (WR) or International Health Department J (IHD-J), at a multiplicity of 10 PFU/cell for 1 h on ice to allow the virus to adsorb to the plasma membrane, and they were then washed with minimal essential medium and incubated at 37°C in complete medium.

Preparation of cells for electron microscopy. Cells were fixed at time intervals between 0 and 24 h postinfection (p.i.). For conventional electron microscopy, infected cells were fixed in 0.5% glutaraldehyde–200 mM sodium cacodylate (pH 7.4) for 30 min, washed in 200 mM sodium cacodylate, and postfixed in 1% osmium tetroxide–1.5% potassium ferrocyanide for 60 min at room temperature. The cells were washed in water, incubated in 0.5% magnesium-uranyl acetate overnight at 4°C, washed again in water, dehydrated in ethanol, and embedded flat in Epon. Sections were cut parallel to the surface of the dish. Serial sections were collected onto slot grids, and lead citrate was added for contrast.

Infected cells and isolated IMV particles were prepared as described previously (41) and then used for cryosectioning. Virus or virus-infected cells were pelleted, frozen in 2.1 M sucrose, and stored under liquid nitrogen (37). Thin sections of frozen cells and virus were cut on a Reichert Ultracut S microtome with FCS attachment.

Preembedding immunogold labeling was performed as described previously (40). Briefly, the cells were grown on glass coverslips and fixed in 4% paraformaldehyde (PFA–250 mM HEPES (pH 7.4) on ice for 10 min followed by 8% PFA–HEPES for 10 min on ice and then for 40 min at room temperature. The fixed samples were incubated with the murine monoclonal antibody AB1.1 (anti-D8L) (24) for 60 min followed by rabbit anti-mouse immunoglobulin G and then protein A-gold conjugates (32) and were subsequently processed as described above for conventional electron microscopy.

Preparation of brain sections for thin-section examination. Thin sections were also cut from samples of guinea pig brain cerebellum that was processed for conventional electron microscopy.

Image collection and data processing. All sections were examined in an Omega 912 electron microscope (Zeiss; LEO Electron Microscope Ltd., Oberkochen, Germany) equipped with a Proscan cooled slow-scan charge-coupled device camera (1,024 by 1,024 pixels) and a Dage-MTI model SIT 66 low-light-level camera. This microscope was capable of tilting the specimens in the goniometer by ±60° and was used for the tilt series. To verify the calibration of the microscope, negatively stained catalase crystals (lattice spacing, 8.75 by 6.75 nm; Agar Scientific Ltd.) were used. All digital images were captured with the integrated Soft Imaging Software (SIS) image analysis package (Soft Imaging Software, GmbH, Münster, Germany), and absolute measurements were recorded directly from the images. Fast Fourier transforms (FFT) and inverse FFT were calculated by using built-in analytical functions of the SIS software package.

Statistical analysis. Numerical values are presented as means ± standard deviations (n = 10) unless stated otherwise. Student's t test was used to test for the significance of the results ($P < 0.01$).

RESULTS

Measurement of organelle and viral membrane thickness in Epon sections. It had been proposed that the IMV surface contains two membranes that are too tightly apposed to be visible (28, 34). If this were true, the thickness of the double membrane would still be twice that of a single membrane. Therefore, we made careful measurements of the thicknesses of cellular membranes from different compartments and compared these to the thicknesses of the membranes of virus crescents and IV and IMV particles. Analysis of host cell membranes and the membranes of IV and IMV within the same cell, processed and measured in the same section, ensures the validity of comparisons between host and viral membranes.

Using a conventional heavy-metal-based positive-contrasting procedure, the thicknesses of membranes from a range of organelles in Epon-embedded sections of VV-infected cells were determined accurately, employing digital-image capture for quantitative analysis (Fig. 1). An entire cell, containing virus factories on either side of the nucleus and maturing virus particles, is shown in Fig. 1A, confirming that the infection was successful. A low-light-level silicon intensifier tube camera was used to acquire high-magnification (up to ×250,000) images of membranes of the nuclear envelope, rough ER, Golgi cisternae, mitochondria, and plasma membrane (Fig. 1B to F). (For details on microscope calibration, see Fig. 4.) Each of these membranes, when cut perpendicular to the electron beam, displayed a distinct trilaminar profile and gave mean values for membrane thickness of close to 5 nm (Table 1). We conclude, therefore, that the thickness of the normal lipid bilayer surrounding cells and cellular organelles measures 5 nm by our fixation and preparation techniques for conventional electron microscopy.

Measurements of the trilaminar profiles of crescent membranes and IV membranes in the same sections shown in Fig. 1 were also made (for examples of micrographs of these virus structures, see Fig. 3, 4, 6, and 7). The thickness of the IV membrane was 5.04 ± 0.24 nm, identical to that of host cell organelle membranes within the measurement error limits of the technique (Table 1). The hypothesis that the thicknesses of these virus and cellular membranes were different was rejected upon statistical analysis of these data.

The outer protein spicules of the IV membrane measured 8.36 ± 0.35 nm, which is too thick for a lipid bilayer.

Measurement of organelle and viral membrane thicknesses in thawed frozen sections. As a complementary approach, we examined the membranes of IV within infected cells and pellets of isolated, fixed IMV by the thawed frozen section technique (37) (Fig. 2). Here the lipid bilayer was characterized by negative contrast. Heavy metals are excluded from the periphery of the polar regions of the phospholipid molecules, causing the lipid bilayer to appear electron translucent. In close agreement with the results of conventional electron microscopy, the membrane of the IV within a viral factory (Fig. 2A) appeared as a 5.37- ± 0.45-nm-thick electron-translucent profile (white) with a 9.30- ± 0.56-nm-thick coating of spicules on the convex surface. Measurements acquired from images of isolated IMV particles (Fig. 2B and C) confirmed that the outer electron-translucent region is also 5.47 ± 0.54 nm thick, with a 9.21- ± 0.67-nm coating on the outer surface. It was also clear that the thawed frozen section technique reveals more detail of the core in isolated IMV particles (Fig. 2B and D) than can usually

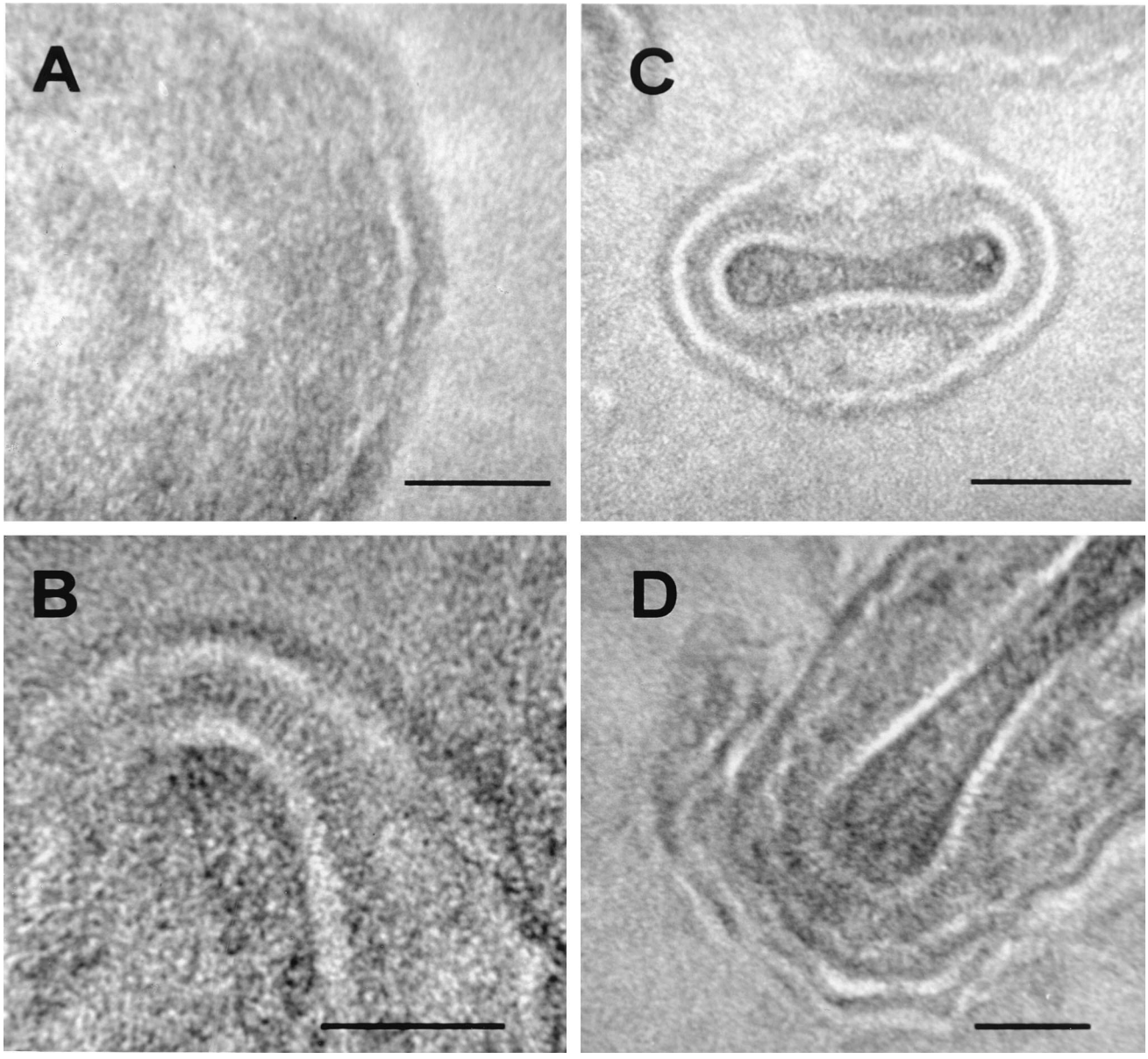

FIG. 2. Viral and cellular membranes observed by the thawed frozen section technique. (A and D) HeLa cells were infected with VV strain WR for 9 h, fixed in PFA, and processed for ultrathin sectioning and contrasting. (A) Shown is an IV particle within a viral factory. The single electron-translucent membrane (white) is covered by a layer of spicules on the convex surface. (B and C) Additional detail is evident in frozen sections of isolated purified IMV particles. The core can be seen to be covered with a periodic palisade of viral proteins, with a thickness of approximately 18 nm, attached to a 8-nm-thick electron-translucent layer. Two electron-translucent zones can be observed in panel B; the inner zone within the particle is part of the core. (D) The two additional cellular membranes acquired by some IMV as they become wrapped by intracellular cisternae to become IEV. Bars, 50 nm (A, B, and D) and 100 nm (C).

be observed by conventional electron microscopy. In addition to the outer membrane of the IMV particles, a characteristic central electron-translucent region was apparent. This was determined to be 8.47 ± 0.79 nm thick, statistically indistinguishable in thickness from the protein spikes on the convex surface of the virus crescents and too thick to be a conventional membrane. This layer was surrounded by 17.19- ± 0.82-nm-long projections (palisade) on its surface (Fig. 2C). Overall, this structure resembles the viral core as described by Dubochet et al. (10). Figure 2D shows an IMV particle being wrapped by cellular membranes to form an IEV, and the two distinct membranes are visible.

Virus crescents contain only one lipid bilayer. To see clearly the morphological details of the IV membrane, it is necessary to have the membrane perpendicular to the electron beam. This can be achieved by tilting the section within the microscope, as illustrated in Fig. 3. The first distinctive structures of assembling virions within the viral factories are the crescent-shaped membranes, which have a brushlike array of electron-dense spicules on their convex surface (5, 19) (Fig. 3). When the membrane of a developing IV particle was not perpendicular to the electron beam (e.g., Fig. 3D), the crescent-shaped membrane had an indistinct outline (oblique section). However, when the specimen was tilted by 20° increments in either

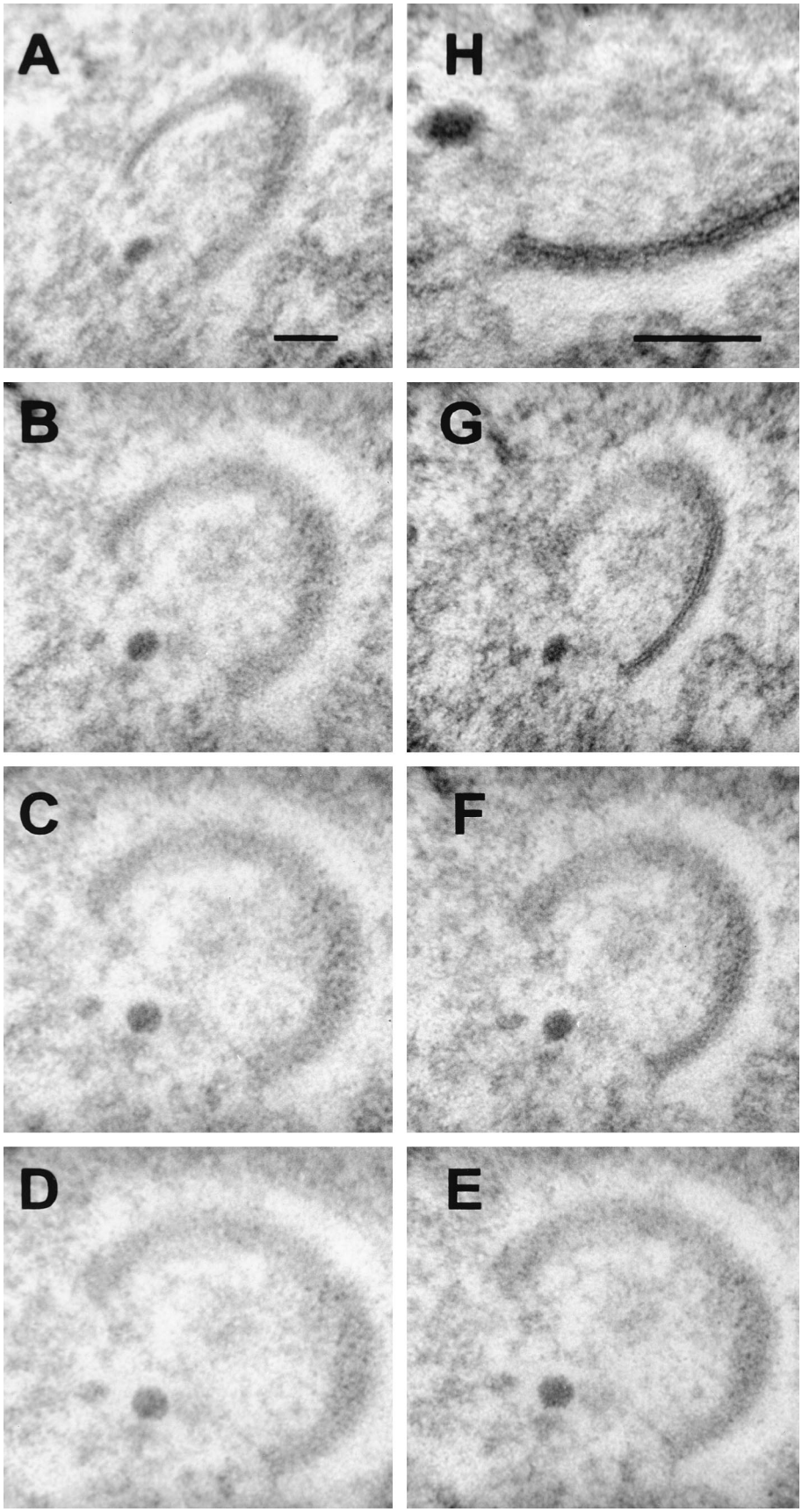

FIG. 3. Tilt series analysis of a forming IV particle. HeLa cells were infected with VV strain WR, and at 16 h p.i., the cells were processed for conventional electron microscopy as described in Materials and Methods. (D) A single virus crescent is shown for which the plane of the membrane is not perpendicular to the incident electron beam. (A to G) Tilting the section through 20° increments identified two positions, −60° (A) and +60° (G), at which the trilaminar structure of part of the single lipid membrane becomes apparent. (H) At a higher magnification, the membrane is seen to be covered on the convex surface by a layer of spicules. Bars, 50 nm.

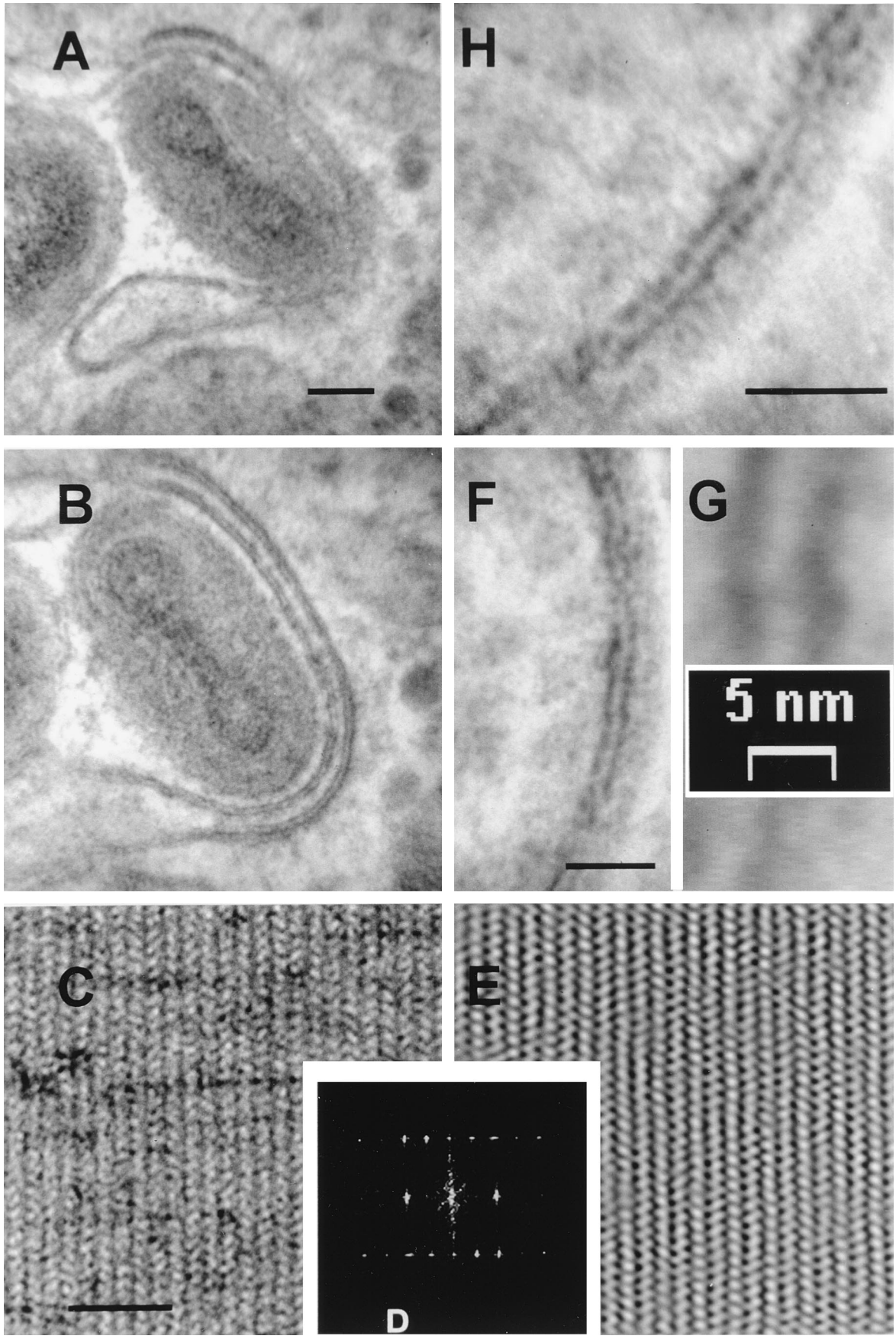
A
H
B
F
G
5 nm
C
E
D

direction, different regions of the single trilaminar profile appeared when the membrane became perpendicular at two positions (Fig. 3A and G). At this tilt angle, the spicules on the convex surface of this membrane were observed clearly (Fig. 3H). At no angle were two trilaminar membranes visible, nor was the crescent-shaped membrane seen to be continuous with cellular membranes.

During the subsequent development of the virus, the IMV becomes wrapped by a double-membraned cisterna (13, 15, 25) (Fig. 2D and 4A and B) to yield an IEV. Like the IMV membrane, the IEV membranes also were clearly visible only when they were perpendicular to the electron beam, so that the trilaminar profile of each membrane and the electron-translucent region between them was apparent (compare, for example, Fig. 4A and B).

For high-magnification measurements, calibration of the digital cameras was confirmed by using two standard specimens, a 2,160-lines/mm grating and catalase crystals with spacings of 8.75 by 6.85 nm. High-magnification images were acquired from the catalase crystal (Fig. 4C) and processed by FFT (Fig. 4D); the measured dimensions for the spacing were 8.51 by 6.55 nm. Since the standard catalase crystal has dimensions of 8.75 by 6.85 nm, the microscope was accurate at this resolution to within ±4%. Selective filtering of the FFT permitted the inverse calculation (Fig. 4E). Electronically, the final image could be increased to a magnification of 2.8×10^6 without loss of calibration (Fig. 4F and G).

As a result of these calibrations, it was possible to take measurements on digital images with a pixel resolution of 1.53 Å. Analysis of the IV surface under these circumstances identified only one lipid bilayer, measuring 5.04 ± 0.24 nm (Table 1); the presence of two tightly apposed membranes, which should give a thickness of at least 10 nm, was not evident. The layer of electron-dense spicules was measured as well and was found to be 8.36 ± 0.35 nm thick (Fig. 4H). Under these high-resolution conditions, it was apparent that in IV membranes, tilted to be perpendicular to the electron beam, only one lipid bilayer could be detected and measured.

Multiple tightly apposed cellular membranes are still evident at cell junctions and within myelin sheaths surrounding axons. To establish whether it is possible to appose biological membranes so tightly that only a single membrane can be observed in thin-section images, we sought natural examples of tightly apposed membranes. Two specialized regions within normal cells where membranes become tightly apposed have been examined. First, at junctional complexes, the plasma membranes of two adjacent cells are held together tightly by a proteinaceous complex (3). Yet, in plastic-embedded thin sections, it is evident that each lipid bilayer remains distinct under these conditions (Fig. 5A and B). Second, the myelin sheath surrounding axons contains numerous layers of membrane wrapping around the axon. Examination of thin sections of guinea pig brain tissue showed that these membranes are apposed extremely tightly, so that each membrane, but not the normal trilaminar structure, is observed easily (Fig. 5C). However, the size of the area contrasted by the heavy-metal-binding polar regions of the phospholipids is increased. Using image analysis to measure the horizontal mean intensity profile at a high magnification (Fig. 5D), the periodicity for each separate membrane was measured from peak to peak (Table 2). This analysis showed that the lipid bilayers retained their normal dimensions and morphology and still had a measured thickness of 5 nm. These examples demonstrate that when two or more membranes become tightly apposed, they remain as separate entities and are visible and measurable by transmission electron microscopy. Therefore, the failure to see two membranes on the virus crescent, IV, or IMV is evidence that the IMV contains only one membrane.

When many IV particles are formed within viral factories, the single membrane of the forming IV can be seen occasionally to separate from the spicules on the convex surface (Fig. 6F). This phenomenon had been observed in streptolysin O-perforated infected cells that had been treated with protease and was interpreted as being due to the separation of two tightly apposed membranes (34). From our images it is evident that only the inner layer of the two profiles has the characteristic trilaminar appearance of a membrane (Fig. 6F). The outer layer lacks a trilaminar appearance and is contiguous with the spicules that become associated with the membrane again further around the circumference of the IV particle. This separation could be observed in normal infected cells and did not require prior protease treatment, although such treatment might increase the frequency of this detachment.

Virus crescents lack continuity with cellular membranes. In any single section examined by electron microscopy, separate membrane-bound structures can appear contiguous with one another if their membrane boundaries are lost optically within the section. As infection progresses, more spherical IV particles are formed within the viral factories and the available space becomes more crowded. When this happens, separate IV particles can appear superimposed on one another; for instance, three aligned crescents are visible in Fig. 6A, but a higher magnification shows that two such crescents each have a single trilaminar lipid bilayer (Fig. 6B). Especially at the periphery of viral factories, IV profiles may appear to be in continuity with cellular membranes, such as those of mitochondrial (Fig. 6C) or tubular (Fig. 6D) membranes. However, these images do not demonstrate membrane continuity, as illustrated by tilting the specimen shown in Fig. 6D by 20°. The thin tubular membrane that appeared joined to the IV in Fig. 6D is now seen to lie between two IV particles rather than being continuous with either of them (Fig. 6E).

Serial-section analysis is the best method to prove or disprove the existence of any continuity, and this technique was used to examine additional crescent-shaped membranes and IV particles embedded in Epon. This revealed that these structures have no continuity, in three dimensions, with any preexisting cellular membranes, such as the rough ER or IC (Fig. 7). If IV were formed by continuity with cellular membranes, each crescent should be seen by this analysis to have such continuity. However, serial-section examination of 22 virus crescents at various stages of assembly showed that none exhibited conti-

FIG. 4. High-resolution analysis of VV membranes. (A and B) Tilt series analysis of wrapping of IMV by membrane cisternae. HeLa cells were infected with VV strain WR, and at 16 h p.i. they were embedded in Epon and processed for thin-section transmission electron microscopy. The membrane is shown at an oblique angle at a 0° tilt (A) and at a 20° tilt (B). (C to E) Microscope calibration. To verify the calibration of the electron microscope, images of a catalase crystal (a known standard with 8.75- by 6.85-nm lattice spacing) (C) were analyzed with the SIS analysis package linked directly to the electron microscope; the FFT (D) was calculated (D), and the inverse FFT was recalculated, with selection for the diffraction spots at 8.51 and 6.55 nm (E). A digital image (magnification, ×250,000) (F) was zoomed electronically to a magnification of the primary image of 2.8×10^6 (G), in which the SIS-calibrated scale bar was burned into the image and zoomed. (H) At a higher magnification (×500,000), when the IV membrane was perpendicular to the electron beam, only a single trilaminar membrane was observed. At a magnification of ×500,000, each pixel on the digital image is 1.53 Å; typically the membrane measures 32 pixels wide, equivalent to 5 nm. Bars, 50 nm (A to E) and 25 nm (H).

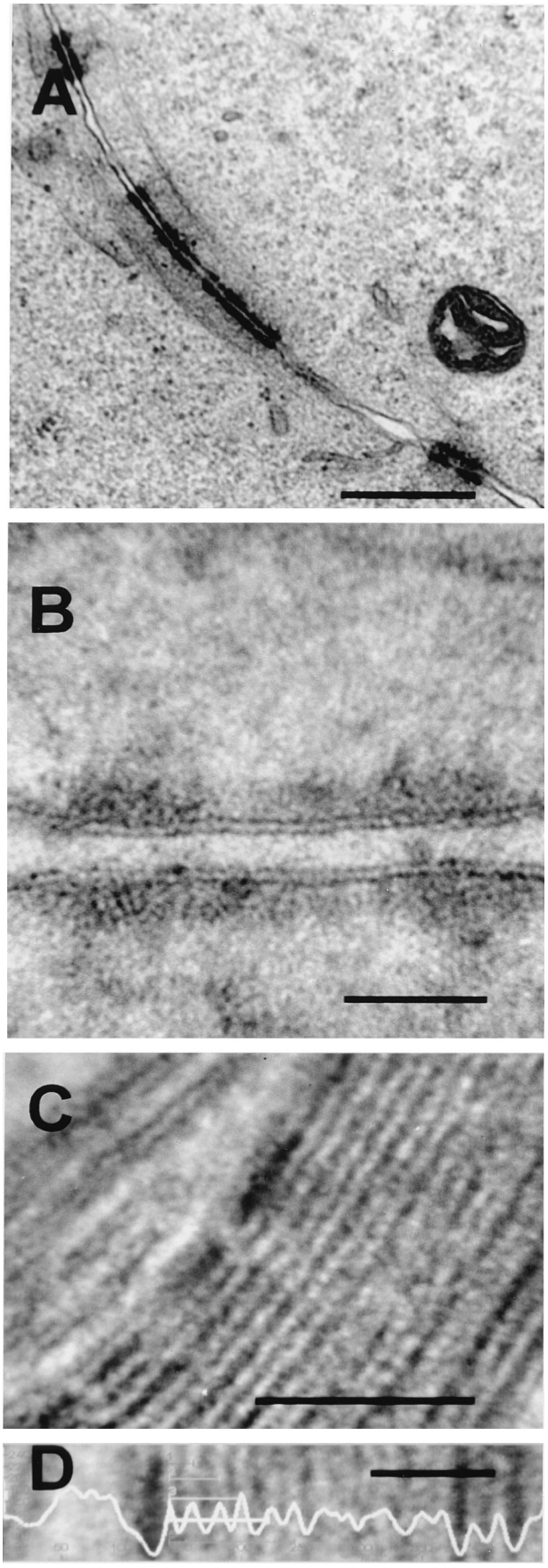

TABLE 2. Dimensions of unit membranes in myelin sheath

Measurement no.	Peak-to-peak maximum (nm) of:	
	Black pixels	White pixels
1	4.87	4.87
2	5.36	6.08
3	4.39	4.39
4	6.33	4.87
5	4.39	5.36
Mean ± SD	5.07 ± 0.81	5.11 ± 0.64

nuity with cellular cisternae. While it is conceivable that continuity might be missed in some cases, the lack of continuity in all virus structures examined makes it most unlikely that these connections exist.

Virus crescents can form at sites remote from IC membranes. The IC is by definition between the ER and the Golgi cisternae, a region of the mammalian cell in culture that is very complex and in which it is difficult to distinguish different membrane compartments. It was proposed that the two membranes of the IC becomes tightly apposed and form the typical crescent-shaped membranes of the IV particles in viral factories (34). Three observations argue against the IC being the source of virus crescents within the cytoplasm. First, shortly after infection, the earliest morphological change within the cell is the appearance of the viral factory (Fig. 8A), which is surrounded characteristically by ER but from which cellular organelles and ribosomes are excluded. Typically, the first crescent-shaped membranes are seen in the center of these large globular viral factories (Fig. 8A), a region deficient in cellular membranes. Second, viral factories can form at sites remote from clusters of Golgi membranes, as shown in Fig. 1A, in which a factory is seen on the opposite side of the nucleus, and as reported previously in growth cones of neuroendocrine cells (38), where IC membranes are not available. These viral factories still contain crescent-shaped membranes. Third, and most definitive, we have observed cases in which formation of crescents and IV particles occurred within the nucleus of an infected cell (Fig. 8B to D), where there is no possibility of continuity with IC membranes. These IV particles are morphologically indistinguishable from the IV particles formed within cytoplasmic viral factories. Although the formation of these nuclear crescents and IVs is rare, the fact that they occur at all provides compelling evidence that membranes of the IC are not required for IV formation.

IMV absorption and entry of viral cores. The presence of a single lipid membrane on the IMV particle resolves the topological problem associated with the uncoating of virions with multiple surface membranes. Instead, a one-to-one fusion event would deliver the virus core into the cytoplasm. To analyze the entry of IMV particles, these virions were allowed to

FIG. 5. Tightly apposed cellular membranes at cell junctions (A and B) and in myelin sheaths around axons (C) remain discernible as individual trilaminar membranes. (A and B) HeLa cells were infected with VV strain WR, and at 24 h p.i. they were processed for electron microscopy as described in Materials and Methods. Images show a junction between cells. (C and D) Sample of guinea pig brain tissue processed for conventional electron microscopy, showing the myelin sheath surrounding the axon of a neuron. (D) Using image analysis (horizontal mean intensity profile) on a portion of the section shown in panel C, the periodicity between lipid bilayers remains 5.07 ± 0.81 to 5.11 ± 0.64 nm. See Table 2 for measurements of peak-to-peak distances. Bars, 500 nm (A), 50 nm (B and C), and 25 nm (D).

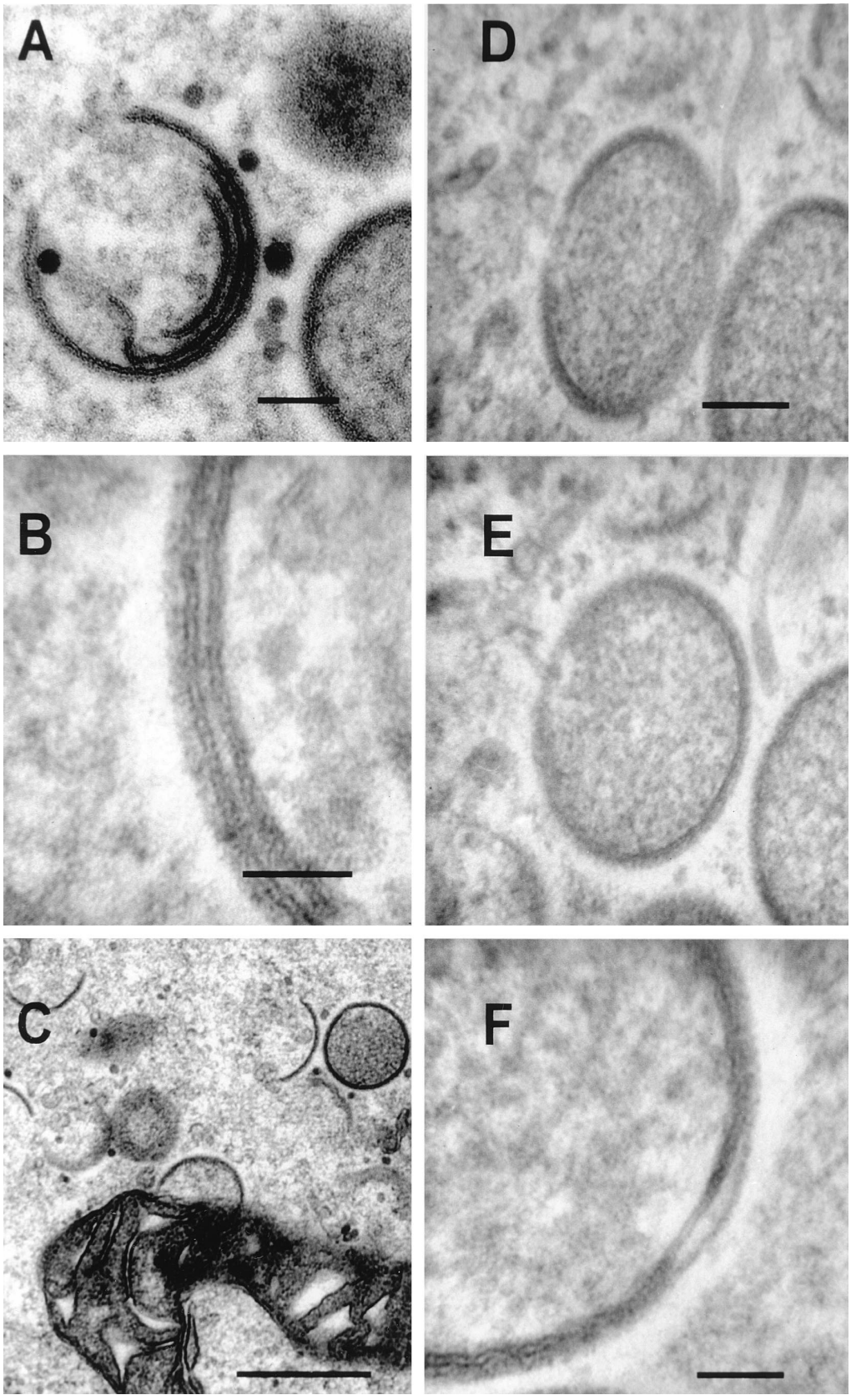

FIG. 6. IV membranes are not continuous with cellular membranes. HeLa cells were infected with VV strain WR (A to E) or IHD-J (F) and were processed for conventional electron microscopy at 16 to 24 h p.i. (A to E) or 16 p.i. (F). (A) Three membranes are encapsulated within the same forming IV particle. (B) When two such membranes are closely apposed, each lipid bilayer can be observed clearly. (C to E) There is apparent continuity of IV membrane with a mitochondrial membrane at the periphery of a virus factory (C) and with the tubular membrane (D) (top right), the latter being lost after tilting the specimen by 20° (E). (F) Occasionally the forming IV membrane can be observed to be disrupted; the inner single membrane has separated from the layer of spicules on the convex surface. Bars, 100 nm (A, D, and E), 50 nm (B and F), and 500 nm (C).

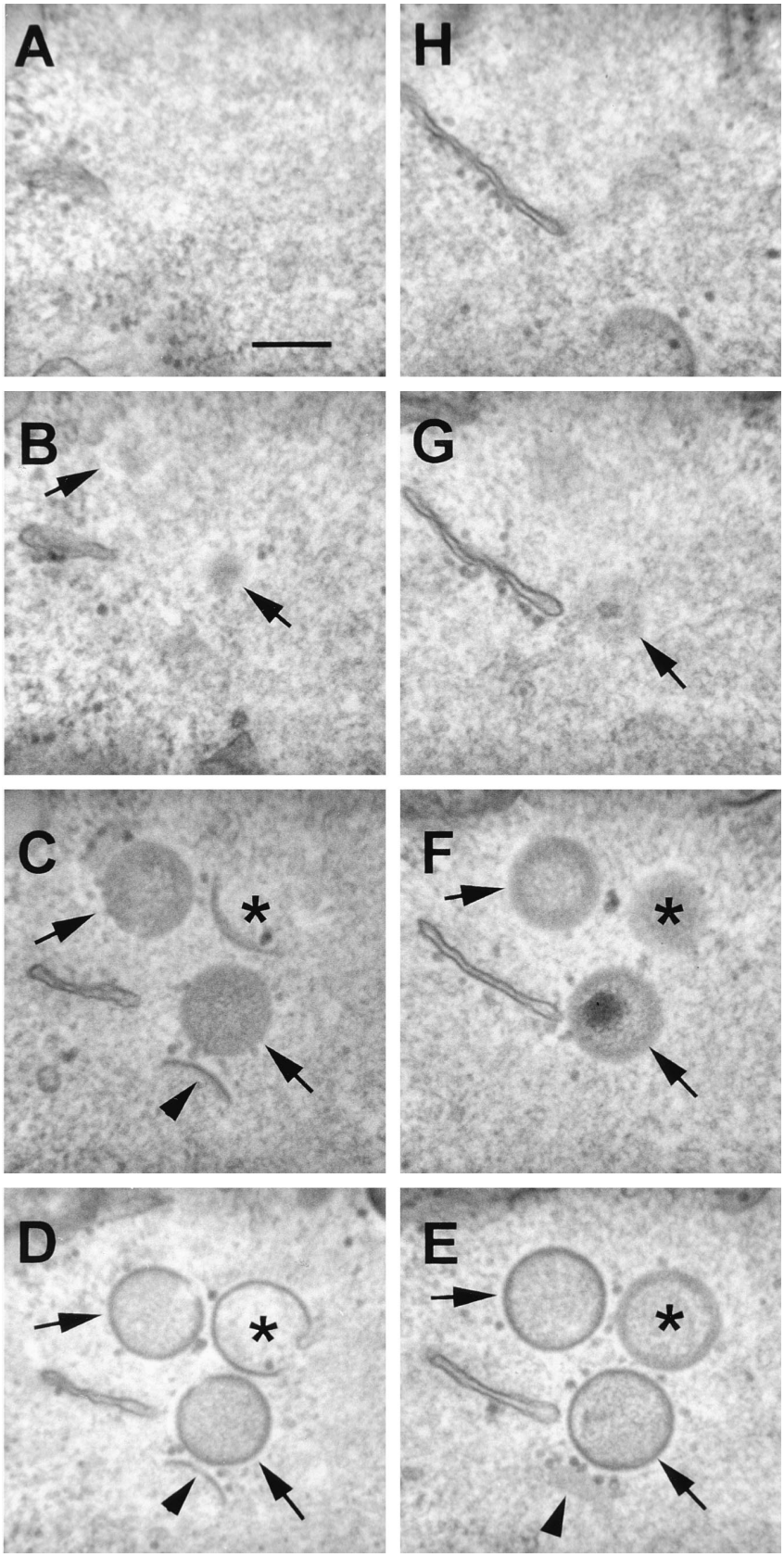

FIG. 7. Serial-section analysis demonstrating a lack of continuity of the membrane forming the IV particles within the viral factories with any preexisting cellular membranes. HeLa cells were infected with VV strain WR, and at 16 h p.i. the cells were processed for serial-section analysis using conventional electron microscopy. Shown are 60-nm-thick serial sections through a virus factory. The arrowheads point to the first crescent-shaped convex membranes with spicules that form in the viral factory. Note that at these first stages of development there is no continuity between the forming ends and cellular membranes. Asterisks indicate larger spherical structures derived from the earlier crescents and which appear closed in some section planes (E and F) but are still forming in other section planes (C and D) with no continuity with any cellular membrane. Other profiles are of fully formed spherical IV particles (arrows). Bar, 200 nm.

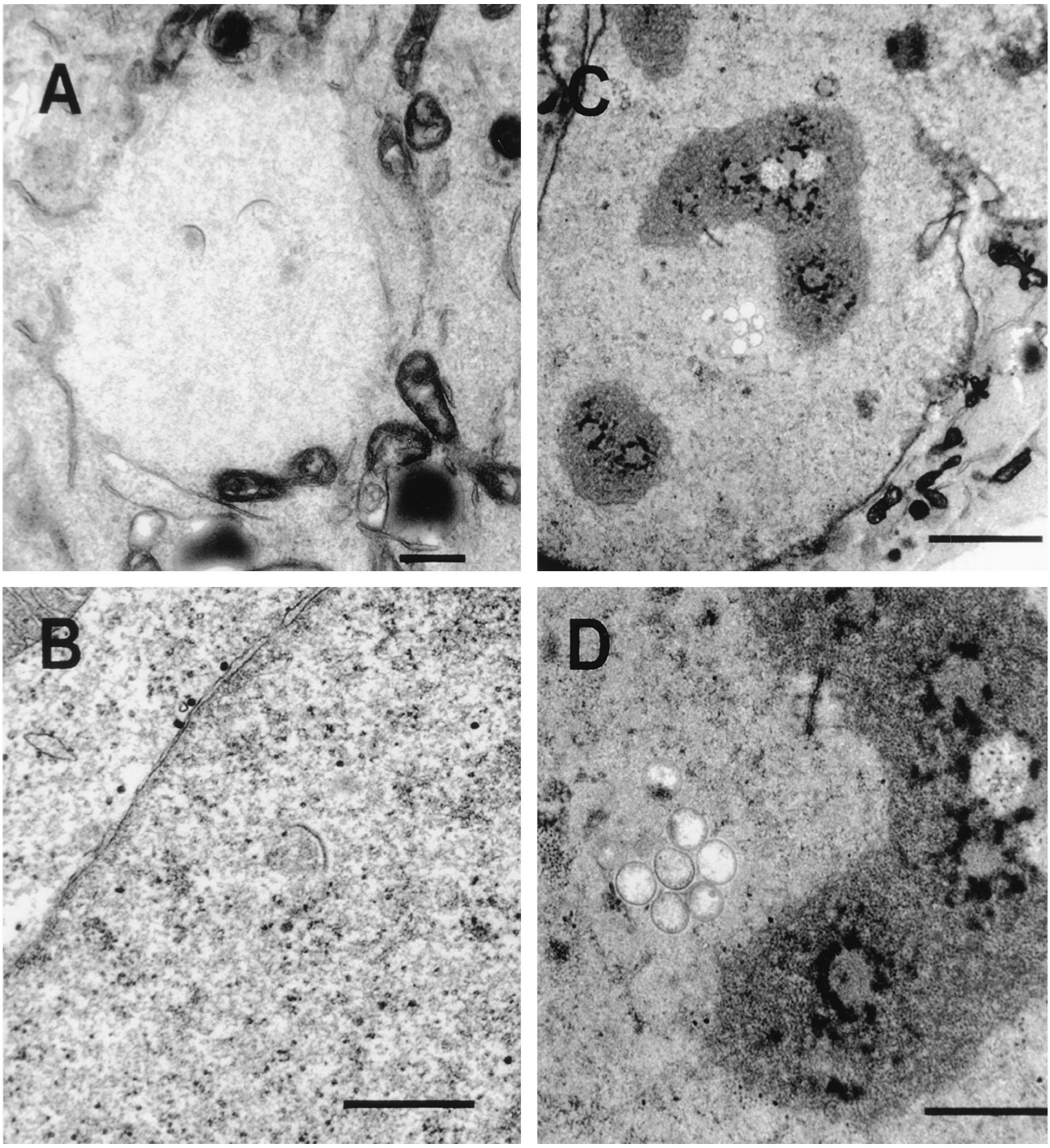

FIG. 8. Presence of virus crescents and IVs in the nucleus. HeLa cells were infected with VV strain WR, and at 16 h p.i. they were processed for conventional electron microscopy. (A) A virus factory in the cytoplasm is electron translucent (pale), and the exclusion of most cellular organelles and the formation of virus crescents deep within the factory are evident. (B to D) Crescent-shaped membranes and IVs within the nucleus. In panel B, the cytoplasm is at the top left and the virus crescent is visible clearly within the nucleoplasm (bottom right). These early virus structures within the nucleus appear indistinguishable from those present within cytoplasmic factories. Bars, 500 nm (A and B) 2,000 nm (C), and 1,000 nm (D).

bind to cell surface receptors at 4°C and were then either immediately fixed (Fig. 9A) or shifted to 37°C for 10 to 20 min prior to fixation (Fig. 9B to D). After fixation, each sample was labelled with antibody to the D8L surface protein of IMV. At 4°C, the antibody–protein A-gold complex labels the complete circumference of the viral particle (Fig. 9A). After a short period of incubation at 37°C, the IMV particles become associated tightly with the plasma membrane, similar to the phagocytic zippering seen in macrophages. The antibody–protein A-gold complex then has access only to the exposed surfaces of

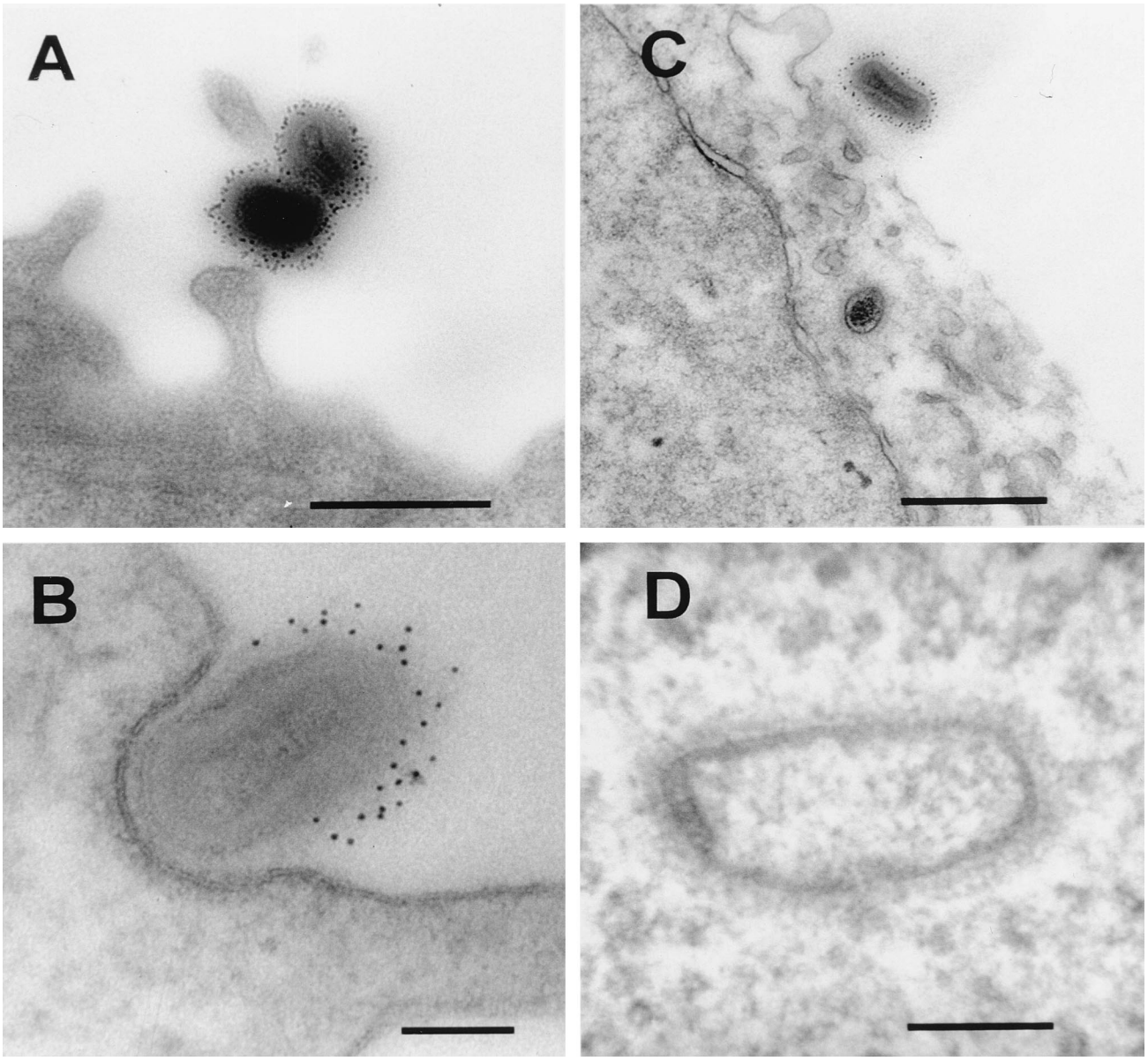

FIG. 9. Viral binding and entry into RK_{13} cells. (A) Purified IMV particles were bound to the cell surface (100 PFU/cell) at 4°C and were labelled by the preembedding technique with antibodies to D8L. (B to D) IMV particles were bound to cells as for panel A, and the cells were shifted to 37°C for 20 min and then treated as for panel A. (B) Note that when IMV particles become engulfed tightly within a pocket of the plasma membrane, the anti-D8L antibodies are excluded. (C and D) Some IMV particles have fused with the cell membrane and released the viral core into the cytoplasm. (D) Note that the distinctive core in the cytoplasm appears to have expanded but retains a fuzzy coat measuring about 18 nm. Bars, 500 nm (A and C) and 100 nm (B and D).

the viral particles (Fig. 9B). This stage is considered to precede fusion at the plasma membrane rather than complete phagocytosis (39). At this early time, viral cores, but not intact IMV particles within vesicles, are evident within the cytoplasm of the cell (Fig. 9C and D). At a high magnification (Fig. 9D), the viral core released into the cytoplasm has a fuzzy coat with a thickness of approximately 18 nm, similar to the internal periodic structures seen in frozen sections of IMV particles. The viral cores observed in the cytoplasm do not have the characteristic trilaminar structure indicative of a membrane at any angle of tilt. This observation is consistent with the demonstration by confocal microscopy that intracellular cores do not stain with antibody directed against the IMV surface (39). The core is apparently delivered into the cytoplasm free of an enclosing membrane by a one-to-one fusion of the IMV and cell membranes.

DISCUSSION

In this study, we demonstrated that the VV IV and IMV surfaces contain only a single lipid bilayer and that this can form without continuity with cellular membranes from the IC. These conclusions are supported by the following observations. (i) Within the same infected cells, the thicknesses of different cellular membranes and the IV membrane are all statistically indistinguishable (close to 5 nm) when measured by high-resolution electron microscopy of Epon-embedded sections. (ii) The thicknesses of the IV and IMV membranes measured

by cryoelectron microscopy were 5.37 ± 0.43 and 5.47 ± 0.54 nm, respectively, and were statistically indistinguishable from each other and from measurements of virus and cellular membranes in Epon-embedded sections. (iii) Tilt series analysis of Epon-embedded thin sections of infected cells showed that when the section was perpendicular to the electron beam only a single trilaminar membrane was evident and that this was covered on the convex surface by a layer of spikes 8.36 ± 0.35 nm thick. (iv) Despite there being only a single visible lipid bilayer in the IV membrane, under the same conditions, very closely apposed cellular membranes in junctions between cells and in myelin sheaths around axons were clearly visible as distinct trilaminar structures. (v) Serial-section analyses of virus crescents provided no evidence of continuity of these crescents with existing cellular membranes. (vi) In cases in which a cellular membrane appeared to overlap or have continuity with a virus crescent, tilt series analysis demonstrated that no continuity existed. (vii) Virus crescents were found to form deep within the center of virus factories (from which cellular membranes are largely excluded) and rarely, but most dramatically, within the nucleus.

These conclusions are consistent with those derived from electron-microscopic studies of the biogenesis of VV in whole-mount preparations and thin sections as reported by Dales and coworkers (5–7) and several other laboratories (12, 17, 19, 38) but are not in agreement with the work of Sodeik et al. (34), who concluded that the IMV coat contains two lipid membranes that are derived from the IC. Evidence supporting the latter model was as follows: (i) the nascent-crescent and IV membranes were reported to be continuous with cellular-membrane cisternae that were considered to be the IC because of immunogold labelling with protein markers for this compartment, (ii) two layers were detected in the surface of IV after treatment with dithiothreitol or protease, and (iii) cryoelectron microscopy provided evidence that the IMV has two membranes.

Is there continuity between cellular membranes and virus crescents? Evidence presented by Sodeik et al. for continuity of cellular-membrane cisternae and virus crescents (34) was in our view unconvincing. In some cases, sections were taken from regions of virus factories in which many crescents or IVs were present, rather than from regions with single, well-separated crescents in isolation. Furthermore, the presented images of cellular membranes that were proximal to virus crescents could not prove continuity because tilt series analyses were not included. As illustrated in this study (Fig. 4), membranes which appear proximal or even continuous may be shown by this technique to be separate. Another important way to address continuity or discontinuity is serial-section analysis. This was not included in the study of Sodiek et al. (34) but was used here and revealed no continuity between cellular membranes and different virus crescents ($n = 22$) (Fig. 7). The formation of virus crescents at sites within infected cells that are remote from IC membranes, such as deep within a factory early during infection, at the side of the nucleus opposite that of the Golgi complex (Fig. 1), at nerve growth cones (38), and within the nucleus, is also inconsistent with a role for IC membranes in crescent formation. Other poxviruses, e.g., the avipoxvirus penguinpox virus, have been reported to form virus crescents within the nucleus (35). Clearly, the formation of morphologically normal crescents at this location rules out a role for IC membranes or other cytoplasmic-membrane cisternae.

Antibodies against proteins specific for the IC were used by Sodeik et al. to investigate the presence of these proteins in membranes adjacent to or continuous with virus crescents, in crescents, and in IV and IMV particles (34). The immunocytochemical data reported for thawed frozen sections should be viewed with caution when addressing the continuity of cellular and virus membranes, because serial-section analysis was not included. Although IC markers were found in cellular membranes, they were not detected in any virus structure. Even IC-specific proteins expressed at much higher levels by VV recombinants were not found in virus structures. Thus, if the IC membrane cisterna was used as the source of the virus membrane, non-VV proteins would somehow be excluded from virus particles. This might be so but is in stark contrast to the results of a study of the incorporation into EEV of cellular proteins derived from wrapping membrane, in which all six proteins that were examined were found in EEV but not IMV (40).

One or two membranes? The evidence by Sodiek et al. (34) for the existence of two membranes in the IMV presented derived partly from studies involving permeabilization of infected cells with streptolysin O followed by protease treatment. The resulting images showed a separation of the IMV membrane into two layers. A similar separation of the IMV surface layers within cells that had not been permeabilized or treated with protease was observed here (e.g., Fig. 6F). Whereas Sodiek et al. (34) interpreted these structures as comprising two lipid bilayers, our interpretation is that the inner layer, which has a thickness (5 nm) and trilaminar morphology that are characteristic of lipid bilayers, represents one membrane while the outer layer, which is 8 nm thick, lacks the trilaminar morphology, and has periodicity, is a protein coat. When IV membranes were in sharp focus, perpendicular to the electron beam, only a single membrane was visible.

Earlier studies using rifampin, an inhibitor of poxvirus morphogenesis, provided evidence for only a single membrane. Rifampin blocks VV morphogenesis prior to formation of crescents and gives rise to rifampin bodies within the cytosol; these bodies contain dense viroplasm surrounded by a membrane (23). However, removal of the drug allows morphogenesis to continue and to be studied in structures synchronized at the same stage of infection. The membrane surrounding rifampin bodies was converted into virus crescents within minutes of rifampin washout (12), and these authors provided very clear electron micrographs showing that the membranes around the rifampin bodies and the virus crescent are continuous and contain a single trilaminar membrane. The former was converted into the latter by first acquiring protein spikes on the outer surface and then developing curvature. Figure 9c of that paper is particularly convincing and shows two crescents linked by a single trilaminar membrane from which the coat of protein spikes are absent (12).

The Epon sections provided by Sodiek et al. (34) showed only a single lipid bilayer in crescents and IVs. The failure to see two lipid bilayers was attributed to their being too closely apposed to be visible (28, 34). To examine the appearance of closely apposed cellular membranes, we have looked at two sites at which such tight apposition normally occurs, cell-cell junctions and the myelin sheath surrounding axons of neurons. At both of these sites, membranes become apposed extremely tightly, but the two unit membranes remain discernible. Furthermore, electron-microscopic imaging of artificial stacked lipid bilayers in the vitrified state after high-pressure freezing still permits clear visualization of each unit membrane (11). Thus, a double trilaminar structure with a thickness of at least 10 nm would be expected if the crescents inside viral factories consisted of two tightly apposed membranes. The appearance of a single trilaminar unit membrane with a thickness of 5 nm

in both crescents and IVs shows that only one membrane exists.

Images of thawed frozen sections were cited as evidence for the existence of two membranes in IMV (28, 34). However, the second structure proposed to be a membrane is well separated from the surface membrane, surrounds the virus core, is covered by an 18-nm-thick layer of spikes (as shown by Dubochet et al. [10] and here [Fig. 2]), and is 8 nm thick. Moreover, when detergents are used to remove lipid from IMVs, the structure of the virion core remains unchanged, exhibiting a characteristic surface palisade of electron-dense protrusions (42). Similarly, treatment of IMV with Nonidet P-40 and dithiothreitol produces particles that are less rounded and smaller than IMV particles, but these particles retain surface spikes that protrude approximately 20 nm (10). These structures are very similar to the surface protrusions visible on cytoplasmic viral cores which have had a lipid bilayer removed physiologically by fusion at the cell surface (e.g., Fig. 9D).

In a later study of VV by cryoelectron microscopy, Roos et al. noted that internal IMV antigens became exposed after treatment of IMV with reducing agents, and this led these authors to postulate that the IMV is surrounded by a discontinuous structure consisting of two tightly apposed membranes in which the discontinuity is sealed by a proteinaceous plug (28). At the site of discontinuity, each double-membrane layer was proposed to overlap. However, numerous authors have published electron micrographs of sections through IV and IMV particles that show these IVs to be complete ovals or brick-shaped structures without regions of membrane overlap (7, 17, 19, 38). It is most unlikely that such membrane overlap would have been missed in every section examined, and the plug, if it existed, would be more likely to be a line of overlap down one side or end, or both, of the particle rather than being a single point.

Biochemical characterization and subcellular localization of viral proteins have also started to contribute to the debate on IMV membrane organization. For example, the 21-kDa cleavage product of the A17L gene (27) has been shown to be essential for the formation of viral membranes (26, 43) and has been localized to crescent membranes and IMV (18, 43). The report that p21 is found in the IC (18) was contradicted by another study (43). The p21 protein has several putative transmembrane domains, and antibody labelling suggests that both the amino (18) and carboxy (18, 43) termini are exposed on the concave side of crescent membranes. The 21-kDa protein interacts directly with a 14-kDa protein (27), and this interaction is essential to recruit p14 to the outer convex surface of the IMV (33). A single-membrane model for virus crescents is compatible with the localization of regions of p21 on both the convex and concave surfaces of the IV crescent, whereas a two-bilayer model cannot easily account for this appearance.

Virus entry. IMV enters cells by fusing with the plasma membrane in a pH-independent manner (2, 9, 16, 39), whereas EEV enters by endocytosis and requires a low pH (14, 39). The presence of only a single membrane in IMV resolves the topological problem of shedding multiple membranes during virus entry into cells, and a single membrane fusion event serves to release the virus core into the cytoplasm, as occurs for other enveloped viruses. Fusion takes place at the plasma membrane for IMV or within the acidified endosomes for IMV released from within EEV by the low-pH-induced disruption of the EEV envelope (39). Morphological examination of IMV entry shows a tight apposition of the IMV membrane with the plasma membrane, sufficient to exclude antibodies against IMV membrane proteins, followed by the release of a virion core into the cytoplasm (Fig. 9). This core does not have a detectable unit membrane on its surface, even when the specimen is tilted to look for the characteristic trilaminar organization of a lipid bilayer (Fig. 9).

In conclusion, our data are consistent with a model in which the crescents within VV factories contain a single lipid bilayer membrane and VV IMV are surrounded by only a single lipid bilayer membrane. The present study does not address the origin of this single membrane, although it appears that continuity with host organelle membranes can be excluded. Finally, the close similarity of electron micrographs documenting the morphogenesis of poxviruses from different genera (8, 20, 29) and even subfamilies (36) suggests that these viruses all have the same number of membranes that are formed in similar ways, as proposed previously (36).

ACKNOWLEDGMENTS

We thank Christopher M. Sanderson for helpful discussion and critical reading of the manuscript and Lance Tomlinson for expert photographic work.

Alain Vanderplasschen is a permanent senior research assistant of the Fonds National Belge de la Recherche Scientifique (F.N.R.S.) at the University of Liège, Liège, Belgium. This work was supported by a programme grant from the United Kingdom Medical Research Council (PG8901790) and an equipment grant from The Wellcome Trust (039155/Z/93/1.2).

REFERENCES

1. **Blasco, R., and B. Moss.** 1991. Extracellular vaccinia virus formation and cell-to-cell virus transmission are prevented by deletion of the gene encoding the 37,000-Dalton outer envelope protein. J. Virol. **65:**5910–5920.
2. **Chang, A., and D. H. Metz.** 1976. Further investigations on the mode of entry of vaccinia virus into cells. J. Gen. Virol. **32:**275–282.
3. **Cross, P. C., and K. L. Mercer.** 1993. Cell and tissue ultrastructure: a functional perspective. W. H. Freeman and Co., New York, N.Y.
4. **Cudmore, S., P. Cossart, G. Griffiths, and M. Way.** 1995. Actin-based motility of vaccinia virus. Nature **378:**636–638.
5. **Dales, S., and E. H. Mosbach.** 1968. Vaccinia as a model for membrane biogenesis. Virology **35:**564–583.
6. **Dales, S., and B. G. T. Pogo.** 1981. Biology of poxviruses, vol. 18. Springer-Verlag, Berlin, Germany.
7. **Dales, S., and L. Siminovitch.** 1961. The development of vaccinia virus in Earles L strain cells as examined by electron microscopy. J. Biophys. Biochem. Cytol. **10:**475–503.
8. **deHarven, E., and D. S. Yohn.** 1966. The fine structure of the Yaba monkey tumor poxvirus. Cancer Res. **26:**995–1008.
9. **Doms, R. W., R. Blumenthal, and B. Moss.** 1990. Fusion of intra- and extracellular forms of vaccinia virus with the cell membrane. J. Virol. **64:** 4884–4892.
10. **Dubochet, J., M. Adrian, K. Richter, J. Garces, and R. Wittek.** 1994. Structure of intracellular mature vaccinia virus observed by cryoelectron microscopy. J. Virol. **68:**1935–1941.
11. **Erk, I., G. Nicolas, A. Caroff, and J. Lepault.** 1998. Electron microscopy of frozen biological objects: a study using cryosectioning and cryosubstitution. J. Microsc. **189:**236–248.
12. **Grimley, P. M., E. N. Rosenblum, S. J. Mims, and B. Moss.** 1970. Interruption by rifampin of an early stage in vaccinia virus morphogenesis: accumulation of membranes which are precursors of virus envelopes. J. Virol. **6:**519–533.
13. **Hiller, G., and K. Weber.** 1985. Golgi-derived membranes that contain an acylated viral polypeptide are used for vaccinia virus envelopment. J. Virol. **55:**651–659.
14. **Ichihashi, Y.** 1996. Extracellular enveloped vaccinia virus escapes neutralization. Virology **217:**478–485.
15. **Ichihashi, Y., S. Matsumoto, and S. Dales.** 1971. Biogenesis of poxviruses: role of A-type inclusions and host cell membranes in virus dissemination. Virology **46:**507–532.
16. **Janeczko, R. A., J. F. Rodriguez, and M. Esteban.** 1987. Studies on the mechanism of entry of vaccinia virus in animal cells. Arch. Virol. **92:**135–150.
17. **Joklik, W. K., and Y. Becker.** 1964. The replication and coating of vaccinia DNA. J. Mol. Biol. **10:**452–474.
18. **Krijnse-Locker, J., S. Schleich, D. Rodriguez, B. Goud, E. J. Snijder, and G. Griffiths.** 1996. The role of a 21-kDa viral membrane protein in the assembly of vaccinia virus from the intermediate compartment. J. Biol. Chem. **271:** 14950–14958.
19. **Morgan, C.** 1976. Vaccinia virus reexamined: development and release. Virology **73:**43–58.

20. **Morgan, C., S. A. Ellison, H. M. Rose, and D. H. Moore.** 1954. Structure and development of viruses observed in the electron microscope. II. Development and release. J. Exp. Med. **100:**301–310.
21. **Moss, B.** 1996. Poxviridae: the viruses and their replication, p. 2637–2671. *In* B. N. Fields, D. M. Knipe, and P. M. Howley (ed.), Fields virology, vol. 2. Lippincott Raven Press, New York, N.Y.
22. **Moss, B., and E. N. Rosenblum.** 1973. Protein cleavage and poxvirus morphogenesis: tryptic peptide analysis of core precursors accumulated by blocking assembly with rifampicin. J. Mol. Biol. **81:**267–269.
23. **Moss, B., E. N. Rosenblum, E. Katz, and P. M. Grimley.** 1969. Rifampicin: a specific inhibitor of vaccinia virus assembly. Nature **224:**1280–1284.
24. **Parkinson, J. E., and G. L. Smith.** 1994. Vaccinia virus gene A36R encodes a M(r) 43–50 K protein on the surface of extracellular enveloped virus. Virology **204:**376–390.
25. **Payne, L. G., and K. Kristenson.** 1979. Mechanism of vaccinia virus release and its specific inhibition by N_1-isonicotinoyl-N_2-3-methyl-4-chlorobenzoylhydrazine. J. Virol. **32:**614–622.
26. **Rodríguez, D., M. Esteban, and J. R. Rodríguez.** 1995. Vaccinia virus A17L gene product is essential for an early step in virion morphogenesis. J. Virol. **69:**4640–4648.
27. **Rodriguez, D., J.-R. Rodriguez, and M. Esteban.** 1993. The vaccinia virus 14-kilodalton fusion protein forms a stable complex with the processed protein encoded by the vaccinia virus A17L gene. J. Virol. **67:**3435–3440.
28. **Roos, N., M. Cyrklaff, S. Cudmore, R. Blasco, J. Krijnse-Locker, and G. Griffiths.** 1996. A novel immunogold cryoelectron microscopic approach to investigate the structure of the intracellular and extracellular forms of vaccinia virus. EMBO J. **15:**2343–2355.
29. **Scherrer, R.** 1968. Morphogénese et ultrastructure du virus fibromateux de Shope. Pathol. Microbiol. **31:**129–146.
30. **Schmelz, M., B. Sodeik, M. Ericsson, E. J. Wolffe, H. Shida, G. Hiller, and G. Griffiths.** 1994. Assembly of vaccinia virus: the second wrapping cisterna is derived from the trans Golgi network. J. Virol. **68:**130–147.
31. **Singer, S. J., and G. L. Nicolson.** 1972. The fluid mosaic model of the structure of cell membranes. Science **175:**720–731.
32. **Slot, J. W., and H. J. Geuze.** 1985. A new method of preparing gold probes for multiple-labeling cytochemistry. Eur. J. Cell Biol. **38:**87–93.
33. **Sodeik, B., S. Cudmore, M. Ericsson, M. Esteban, E. G. Niles, and G. Griffiths.** 1995. Assembly of vaccinia virus: incorporation of p14 and p32 into the membrane of the intracellular mature virus. J. Virol. **69:**3560–3574.
34. **Sodeik, B., R. W. Doms, M. Ericsson, G. Hiller, C. E. Machamer, W. van't Hof, G. van Meer, B. Moss, and G. Griffiths.** 1993. Assembly of vaccinia virus: role of the intermediate compartment between the endoplasmic reticulum and the Golgi stacks. J. Cell Biol. **121:**521–541.
35. **Stannard, L. M., D. Marias, D. Kow, and K. R. Dumbell.** 1998. Evidence for incomplete replication of a penguin poxvirus in cells of mammalian origin. J. Gen. Virol. **79:**1637–1646.
36. **Stoltz, D. B., and M. D. Summers.** 1972. Observations on the morphogenesis and structure of a hemocytic poxvirus in the midge *Chrinomus attenuatus*. J. Ultrastruct. Res. **40:**581–598.
37. **Tokuyasu, K. T.** 1980. Immunochemistry on ultrathin frozen sections. Histochem. J. **12:**381–403.
38. **Tooze, J., M. Hollinshead, B. Reis, K. Radsak, and H. Kern.** 1993. Progeny vaccinia and human cytomegalovirus particles utilize early endosomal cisternae for their envelopes. Eur. J. Cell Biol. **60:**163–178.
39. **Vanderplasschen, A., M. Hollinshead, and G. L. Smith.** 1998. Intracellular and extracellular vaccinia virions enter cells by different mechanisms. J. Gen. Virol. **79:**877–887.
40. **Vanderplasschen, A., E. Mathew, M. Hollinshead, R. B. Sim, and G. L. Smith.** 1998. Extracellular enveloped vaccinia virus is resistant to complement because of incorporation of host complement control proteins into its envelope. Proc. Natl. Acad. Sci. USA **95:**7544–7549.
41. **Vanderplasschen, A., and G. L. Smith.** 1997. A novel virus binding assay using confocal microscopy: demonstration that the intracellular and extracellular vaccinia virions bind to different cellular receptors. J. Virol. **71:**4032–4041.
42. **Wilton, S., A. R. Mohandas, and S. Dales.** 1995. Organization of the vaccinia envelope and relationship to the structure of intracellular mature virions. Virology **214:**503–511.
43. **Wolffe, E. J., D. M. Moore, P. J. Peters, and B. Moss.** 1996. Vaccinia virus A17L open reading frame encodes an essential component of nascent viral membranes that is required to initiate morphogenesis. J. Virol. **70:**2797–2808.